Journal of Power Sources 196 (2011) 1006–1011

Contents lists available at ScienceDirect

Journal of Power Sources

journal homepage: www.elsevier.com/locate/jpowsour

X-ray photoemission spectroscopy analysis of N-containing carbon-based cathode catalysts for polymer electrolyte fuel cells

Hideharu Niwa[a], Masaki Kobayashi[a,b], Koji Horiba[a,b], Yoshihisa Harada[a,b], Masaharu Oshima[a,b,*], Kiyoyuki Terakura[c], Takashi Ikeda[d], Yuka Koshigoe[e], Jun-ichi Ozaki[e], Seizo Miyata[f], Shigenori Ueda[g], Yoshiyuki Yamashita[g], Hideki Yoshikawa[g], Keisuke Kobayashi[g]

[a] Department of Applied Chemistry, School of Engineering, The University of Tokyo, 7-3-1 Hongo, Bunkyo-ku, Tokyo 113-8656, Japan
[b] Synchrotron Radiation Research Organization, The University of Tokyo, 7-3-1 Hongo, Bunkyo-ku, Tokyo 113-8656, Japan
[c] Research Center for Integrated Science, Japan Advanced Institute of Science Technology (JAIST), 1-1 Asahidai, Nomi Ishikawa 923-1292, Japan
[d] Quantum Beam Science Directorate, Japan Atomic Energy Agency (JAEA), SPring-8, 1-1-1 Kouto, Sayo-cho, Sayo-gun, Hyogo 679-5148, Japan
[e] Department of Chemical & Environmental Engineering, Graduate School of Engineering, Gunma University, 1-5-1 Tenjin-cho, Kiryu, Gunma 376-8515, Japan
[f] New Energy and Industrial Technology Development Organization, 1310 Omiya-cho, Saiwai-ku, Kawasaki, Kanagawa 212-8554, Japan
[g] National Institute for Materials Science (NIMS), SPring-8, 1-1-1 Kouto, Sayo-cho, Sayo-gun, Hyogo 679-5148, Japan

ARTICLE INFO

Article history:
Received 21 March 2010
Received in revised form 17 August 2010
Accepted 20 August 2010
Available online 19 September 2010

Keywords:
Polymer electrolyte fuel cell
Cathode
Oxygen reduction reaction
X-ray photoemission spectroscopy
Carbon alloy catalysts
Electronic structure

ABSTRACT

We report on the electronic structure of three different types of N-containing carbon-based cathode catalysts for polymer electrolyte fuel cells observed by hard X-ray photoemission spectroscopy. Prepared samples are derived from: (1) melamine and poly(furfuryl alcohol), (2) nitrogen-doped carbon black and (3) cobalt phthalocyanine and phenolic resin. C 1*s* spectra show the importance of sp^2 carbon network formation for the oxygen reduction reaction (ORR) activity. N 1*s* spectra of the carbon-based cathode catalysts are decomposed into four components identified as pyridine-like, pyrrole- or cyanide-like, graphite-like, and oxide nitrogen. Samples having high oxygen reduction reaction activity in terms of oxygen reduction potential contain high concentration of graphite-like nitrogen. O 1*s* spectra are similar among carbon-based cathode catalysts of different oxygen reduction reaction activity. There is no correlation between the ORR activity and oxygen content. Based on a quantitative analysis of our results, the oxygen reduction reaction activity of the carbon-based cathode catalysts will be improved by increasing concentration of graphite-like nitrogen in a developed sp^2 carbon network.

1. Introduction

Catalysts for oxygen reduction reaction (ORR) have been intensively investigated in recent decades for metal–air battery and fuel cell applications [1–19] because of the considerable overpotential with ORR. In particular, the application of the catalysts in polymer electrolyte fuel cells (PEFCs) has attracted much attention and has been demonstrated in vehicular and stationary applications as a new system for the conversion and storage of energy. Conventionally, platinum (Pt) is used as the catalyst on both the cathode and the anode, with higher loading on the cathode due to the sluggish kinetics of ORR in which the oxygen molecule is reduced to water [1]. However the high costs and the scarcity of Pt have obstructed the commercialization of PEFCs. Therefore, ORR catalysts without platinum should be developed.

Among possible replacements for Pt, carbon-based cathode catalysts [2–19] such as carbon alloy catalysts (CACs) [17–19] have been extensively studied owing to their high ORR activities. Carbon alloys are carbon materials modified by other elements such as hydrogen, boron, and nitrogen [20]. Since carbon-based cathode catalysts can be synthesized from a wide variety of materials such as organometallic complexes, iron or cobalt salt, resin, carbon black and ammonia [2–19], there are abundant resources to prepare non-platinum ORR catalysts. The mechanism of the catalytic activity of carbon-based cathode catalysts has long been under debate. It has been suggested that the Me–N_4/C, Me–N_2/C and/or Me–C–N moieties (Me = Co, Fe) act as the ORR active site [2,5–8]. It has also been suggested that nitrogen plays a crucial role in the ORR activity [8,11–18]. In particular, some groups have emphasized the importance of pyridine-like nitrogen as a marker for the edge plane of the carbon layer [8,12,13]. In order to surpass the ability of conventional Pt catalysts, it is important to identify the ORR active

* Corresponding author at: Department of Applied Chemistry, School of Engineering, The University of Tokyo, 7-3-1 Hongo, Bunkyo-ku, Tokyo 113-8656, Japan. Tel.: +81 3 5841 7191; fax: +81 3 5841 8744.
E-mail address: oshima@sr.t.u-tokyo.ac.jp (M. Oshima).

0378-7753/$ – see front matter © 2010 Elsevier B.V. All rights reserved.
doi:10.1016/j.jpowsour.2010.08.054

site in carbon-based cathode catalysts. Hard X-ray photoemission spectroscopy (HXPES) is a powerful tool [21] for determining the chemical state of each constituent element irrespective of surface contamination owing to its large probing depth. In this study, we have prepared three different types of CACs and proposed the origin of the ORR activity in the CACs by investigating the electronic structure of each element in the CACs by HXPES.

2. Experimental methods

2.1. Sample preparation and characterization

Three different types of CACs were synthesized: (1) nitrogen-doped carbon materials prepared by a kneading method in which the precursors contain nitrogen atoms (N1 and N2). N1 and N2 were synthesized from melamine and poly(furfuryl alchol) to have different N-doping levels (N2 > N1). Details of the preparation and the electrochemical characterization of N1 and N2 have been described elsewhere [17]. (2) Nitrogen-doped carbon alloys prepared by an ammoxidation method, where nitrogen is doped onto carbon black (Ketjen Black) with 50% (AO50) and 90% (AO90) ammonia gas at 600 °C. (3) Nanoshell carbon [19] derived from pyrolyzed cobalt phthalocyanine and phenolic resin followed by ball milling. The amount of cobalt in the precursor was adjusted to be 3 wt.% in the mixture of cobalt phthalocyanine and phenolic resin. The temperatures of the pyrolysis were 1000 °C (Co1000). After ball milling, the sample was washed with hydrochloric acid to remove cobalt (Co1000aw).

The ORR activities of these samples were evaluated by rotating disk voltammetry in 0.5 mol L^{-1} H_2SO_4 saturated with oxygen at room temperature [17]. We employed an oxygen reduction potential E_{O2} that is defined as the voltage at which the reduction current density normalized by the area of a glass-like carbon disk electrode reached $-10\ \mu A\ cm^{-2}$ as the ORR activity. The BET specific surface areas were determined by N_2 adsorption measurement at liquid nitrogen temperature with an automatic apparatus (BELSORP 28SA, Japan BEL Co. Ltd.).

2.2. HXPES measurements

The probing depth of HXPES is several times larger than the inelastic mean free paths (IMFPs) of photoelectrons which are approximately 11 nm for the C 1*s*, N 1*s*, and O 1*s* edges and 10 nm for the Co 2*p* edge when the incident photon energy is 5.95 keV [22]. HXPES measurements at BL15XU of SPring-8 were conducted in an ultrahigh-vacuum chamber (base pressure $\sim 3 \times 10^{-7}$ Pa) at room temperature. The photon energy used for the photoemission measurements was approximately 5.95 keV. The overall energy resolution was approximately 0.25 eV. The binding energies were calibrated using the Au 4*f* line. The detection angle of photoelectrons was approximately 1° from the surface normal to gain the detection efficiency. For a detailed chemical analysis, backgrounds of the core level spectra were subtracted by the Shirley method. Each spectrum was fitted with Voigt (Gaussian and Lorentzian) functions, where the Gaussian width was an adjustable parameter, and the Lorentzian width for the N 1*s* and O 1*s* were fixed to 0.25 eV and 0.30 eV, respectively.

3. Results and discussion

3.1. Electrochemical properties

The electrochemical activities for ORR measured by the rotating disk electrode voltammetry are shown in Fig. 1 and Table 1. The BET specific surface areas evaluated by N_2 adsorption are also summarized in Table 1. The three different types of CACs show different profiles of reduction currents in the negative voltage sweep. N1 and N2 have the lowest E_{O2} among all the samples. AO50 and AO90 have similar values of E_{O2}. Although AO50 and AO90 have high surface areas, their ORR activities are lower than those of Co1000 and Co1000aw. Nanoshell carbons (Co1000 and Co1000aw) have similar values of E_{O2}, which is the highest among all the samples. The current density at 0.7 V vs. NHE ($i_{0.7}$) of Co1000aw is larger than that of Co1000, indicating an enhancement of $i_{0.7}$ by the acid washing, while it does not change E_{O2} for Co1000 and Co1000aw.

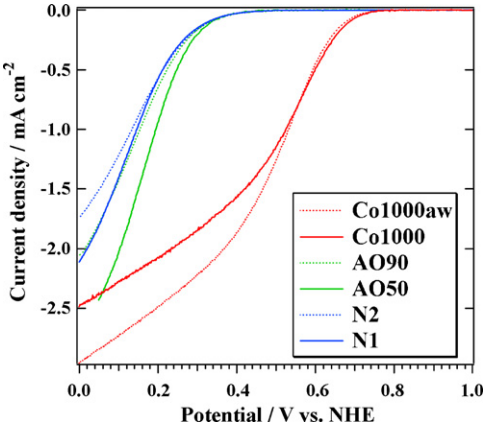

Fig. 1. Voltammograms of the CACs.

3.2. HXPES analysis

3.2.1. Composition ratio of the CACs and Co 2p HXPES

The composition ratios of the CACs calculated from the HXPES data are listed in Table 2. The photoionization cross-section [23] and IMFP [22] are taken into account. The composition ratio of Co in Co1000aw is only 0.03 at. % within the probing depth 10 nm which is sufficiently deep to cover all the area of the nanoshell. According to our recent XANES study, over 80% of the residual cobalt is composed of metallic state [24], while it is known that metallic cobalt

Table 1
Electrochemical activities for ORR measured by rotating disk electrode voltammetry and BET specific surface areas of the CACs.

Sample	E_{O2} [a] (V vs. NHE)	$i_{0.7}$ [b] ($\mu A\ cm^{-2}$)	S_{BET} [c] ($m^2\ g^{-1}$)
Co1000aw	0.75	−49.8	242
Co1000	0.75	−46.4	287
AO90	0.57	–	1200
AO50	0.58	–	1250
N2	0.45	–	122
N1	0.45	–	310

[a] Oxygen reduction potential defined as the voltage at which a reduction current density of $-10\ \mu A\ cm^{-2}$ is reached.
[b] Current densities at 0.70 V vs. NHE ($i_{0.7}$).
[c] BET specific surface area.

Table 2
The composition ratios (at.%) for CACs estimated from the HXPES results. In the calculation of the composition ratios, photoionization cross-section and IMFP at 5.95 keV excitation are taken into account. For AO90, AO50, N2, and N1, there is no cobalt in their precursors.

Sample	C	N	O	Co
Co1000aw	96.33	0.37	3.27	0.03
Co1000	96.48	0.37	3.10	0.05
AO90	97.64	1.07	1.30	–
AO50	95.76	1.85	2.38	–
N2	89.78	1.88	8.34	–
N1	92.07	0.48	7.45	–

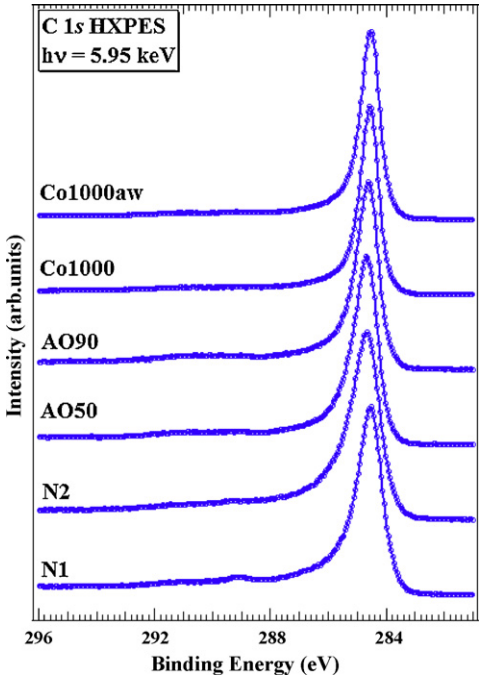

Fig. 2. C 1*s* HXPES spectra of the CACs. Blue dotted lines are the measured data. (For interpretation of the references to colour in this figure legend, the reader is referred to the web version of the article.)

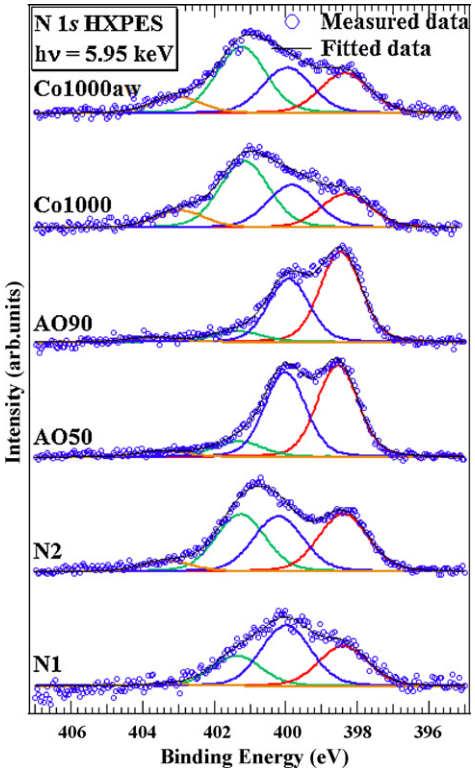

Fig. 3. N 1*s* HXPES spectra of the CACs. Each spectrum is fitted with Voigt functions followed by background subtraction with the Shirley method. Red, blue, green, and orange solid lines are pyridine-like (NP1), pyrrole-like or cyanide-like (NP2), graphite-like (NP3), and oxide (NP4) nitrogen components, respectively. (For interpretation of the references to colour in this figure legend, the reader is referred to the web version of the article.)

is not active for ORR [25]. This result indicates that the residual Co atoms in the CACs do not play an important role in ORR unlike other cases on Co-containing ORR catalysts [6,8]. The detailed discussion about the residual cobalt is described elsewhere [24].

3.2.2. C 1s HXPES

Carbon is the main element present in the CACs, comprising more than 90 at.% in all the samples examined in this study (Table 2). Fig. 2 shows the C 1*s* HXPES spectra of the CACs. The spectra are normalized with respect to the peak height. The peak position and full width at half maximum (FWHM) of each C 1*s* peak at ~284.6 eV are listed in Table 3. The C 1*s* peak energy of each spectrum is within a range of 0.3 eV entered at 284.6 eV, indicating that the CACs predominantly consist of a typical sp^2 carbon network [6,13,26–29]. Among nitrogen-containing carbon-based cathode catalysts, the broad tail toward higher binding energy [30] is attributed to carbon atoms bonded to nitrogen [6,13]. However, it is unlikely that this broad tail is only derived from C–N bonds because the nitrogen content of the CACs is much smaller than the carbon content (see Table 2). Several reports have stated that sp^3 amorphous carbon has a tail that is wider and broader at higher binding energy than typical graphitic sp^2 carbon [28,29]. It is expected that our samples having a broad tail in the C 1*s* HXPES spectra contain predominant sp^3 components such as the CH_3 group or diamond-like C–C bond besides minor C–N bonds. The FWHM of the C 1*s* spectra of Co1000 and Co1000aw are smaller than those of the other CACs, indicating that Co1000 and Co1000aw have more sp^2 carbon network compared with the other CACs. The CAC samples having larger FWHM values (N1, N2, AO50, and AO90) are relatively low ORR active (see Table 1), implying the importance of the carbon structures. It is considered that sufficient sp^2 carbon network formation is necessary for fast electron transfer during ORR.

Considering that the FWHM of the C 1*s* spectra of Co1000 and Co1000aw are quite similar, we can conclude that the acid washing does not drastically change the backbone carbon structure of the CACs unlike carbon nanotubes where the carbon structure seems to be affected by the acid washing [31].

Table 3
Binding energies (eV) and full widths at half maximum (FWHM) (eV) of all CAC samples derived from C 1*s* HXPES spectra.

Sample	Binding energy (eV)	FWHM (eV)
Co1000aw	284.5	0.79
Co1000	284.6	0.76
AO90	284.7	0.91
AO50	284.7	1.02
N2	284.7	1.23
N1	284.5	1.06

3.2.3. N 1s HXPES

Nitrogen content is within 2.0 at.% for each sample (see Table 2). N2 contains more nitrogen than N1, reflecting the nitrogen content in their precursors [17]. Fig. 3 shows N 1*s* HXPES spectra of the CACs. The spectra are normalized to a common area. The profile of the N 1*s* HXPES spectra changes drastically among the samples prepared by different methods. In order to reveal the chemical states of nitrogen in detail, the N 1*s* HXPES spectra are decomposed into four peaks (NP1–NP4) corresponding to different chemical states of nitrogen [26,27,32–34]. The binding energy and relative composition ratio of the four peaks are summarized in Table 4. Peak NP1 around 398.3–398.5 eV is pyridine-like nitrogen neighbouring two carbon atoms in a graphitic sp^2 network [26,32]. The assignment of peak NP2 around 399.9–400.2 eV is controversial; Ray et al. have reported that peak NP2 is cyanide-like nitrogen neighbouring one carbon atom with triple bonds [27], while Pels et al. have claimed that peak NP2 is pyrrole-like nitrogen formed in a five-membered ring [26] as shown in Fig. 4. There could be some

Table 4
Binding energies (eV) of four nitrogen components derived from decomposed HXPES spectra and relative composition ratio (%) of each CAC sample.

Sample	Binding energy (eV)				Relative composition ratio (%)			
	Peak NP1	Peak NP2	Peak NP3	Peak NP4	Peak NP1	Peak NP2	Peak NP3	Peak NP4
Co1000aw	398.4	400.0	401.2	403.0	23.8	27.1	39.5	9.7
Co1000	398.3	399.8	401.2	402.9	21.2	26.7	41.5	10.7
AO90	398.5	399.9	401.3	403.8	52.5	36.8	7.5	3.2
AO50	398.5	400.0	401.3	403.4	45.4	41.9	9.2	3.4
N2	398.4	400.2	401.3	403.3	31.9	30.7	31.6	5.8
N1	398.4	400.0	401.4	403.3	30.1	45.8	22.7	1.4

amount of cyanide-like nitrogen in the CACs since our previous X-ray absorption spectroscopy (XAS) study, which is sensitive to the number of π bonds, has indicated the existence of cyanide-like nitrogen in the CACs heat-treated at 900 °C [35]. Considering that pyrrole-like nitrogen is stable at temperatures as high as 600 °C [26], peak NP2 is a mixture of pyrrole-like nitrogen and cyanide-like nitrogen. Peak NP3 around 401.2–401.4 eV is usually assigned to be graphite-like nitrogen that is hybridized with 3 carbon neighbours in a sp^2 network [32–34]. Peak NP4 around 402.9–403.8 eV is ambiguous; Pels et al. have reported that NP4 possibly corresponds to the nitrogen-oxide of pyridine (as shown in Table 1) or some other oxidized nitrogen functionalities [26]. In this study, NP4 is assumed to be nitrogen bonded to oxygen regardless of its functionalities.

It is found that higher active ORR catalysts such as nanoshell carbons (Co1000 and Co1000aw) have the largest relative composition ratio of NP3 (graphite-like nitrogen) among the four nitrogen components. The result is consistent with our previous XAS study [35]. Comparing atomic composition ratios (Table 2), the nanoshell carbons contain less nitrogen than the other catalysts such as AO50, AO90 and N2 having lower ORR activities, indicating that the total amount of nitrogen is not necessarily correlated with the ORR activity of the CACs; For N1 and N2, the relative composition ratios of NP3 are larger than those for AO50 and AO90, while the ORR activities of N1 and N2 are lower than those of the other CACs. This is probably because N1 and N2 do not have sufficient sp^2 carbon network that helps fast electron transfer during ORR as discussed above by the FWHMs of C 1*s* HXPES. At present, we cannot exclude the contribution of NP4 (nitrogen bonded to oxygen species) to the ORR activity. The N 1*s* spectra of Co1000 and Co1000aw are quite similar, which indicates that the acid washing does not change the chemical state of the nitrogen.

The detailed ORR mechanism is discussed below. The adsorption process of an oxygen molecule is important because it is the first step of ORR [16,36,37]. It has been reported that carbon at the zig-zag edge itself (not neighbouring a nitrogen atom) is active to oxygen adsorption [36]. This is probably because carbon at the zig-zag edge has sharp density of states near the Fermi level called "the edge states" [38], which is crucially important for oxygen adsorption [39]. Other researchers have reported that nitrogen substitution at the zig-zag edge leads to an impurity state near the Fermi level [40]. Ikeda et al. also have shown by a first principle simulation that a carbon atom next to a graphite-like nitrogen at the zig-zag edge tends to adsorb oxygen molecules much easily than a carbon atom not neighbouring a nitrogen atom does [36], in other words, the presence of graphite-like nitrogen at the zig-zag edge enhances the ORR activity. This is consistent with our experimental result that the highly active nanoshell carbons contain much graphite-like nitrogen components, i.e., it is possible that the presence of graphite-like nitrogen at the edge contributes to the ORR activity in carbon catalysts.

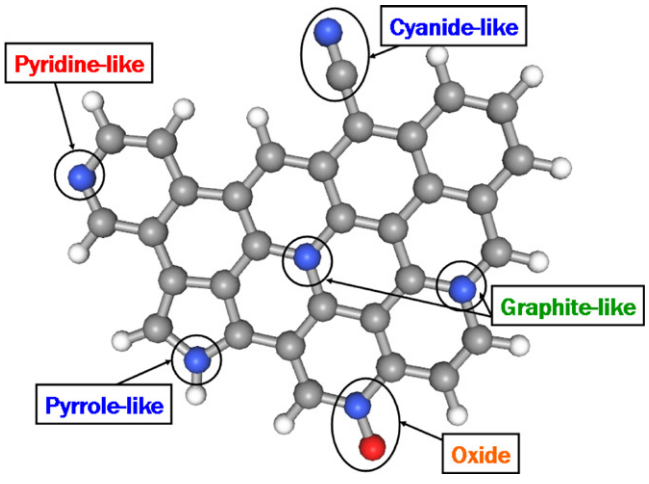

Fig. 4. Schematic of various nitrogen components in N-doped graphene.

3.2.4. O 1s HXPES

The oxygen content varies among the samples (see Table 2). Fig. 5(a) shows the O 1*s* HXPES spectra of the CACs. The spectra are normalized with respect to the peak height. The shapes of the spectra look relatively similar, in spite of the presence of oxygen in different chemical states in the precursors and the different values of E_{O2} of the CACs. It appears that there is no correlation between the oxygen content and E_{O2}. Using Voigt functions, the O 1*s* spectra are nicely fitted to three components (peak OP1–OP3), indicating the presence of at least three oxygen components in the CACs; The C=O group appears around 531.2–531.6 eV (peak OP1), the C–OH and C–O–C groups appear around 532.2–533.4 eV (peak OP2), and chemisorbed oxygen or water appears around 534.6–535.4 eV (peak OP3) [41,42]. Besides, it has been reported that a cobalt oxide peak corresponding to non-stoichiometric cobalt oxide appears around 530.7–531.6 eV (peak OP1) [43]. The O 1*s* HXPES spectra of Co1000 and Co1000aw are different in the lower binding energy region as shown in Fig. 5(b). This suggests that acid washing reduces the lower binding energy component (peak OP1) corresponding to the C=O groups or non-stoichiometric cobalt oxides [41–43]. As the acid washing does not change the ORR activity of the CACs, C=O groups or non-stoichiometric cobalt oxides are not the ORR active site.

3.2.5. Estimation of active site density

In order to quantitatively examine the possibility of nitrogen serving as the active site of ORR, the active site density of the CAC is compared with a conventional 20 wt.% Pt/C cathode catalyst for a PEFC. Here, the active site density is defined as an atomic percentage of the active site in a catalyst. Assuming that all graphite-like nitrogen (designated as peak NP3 in the N 1*s* spectra) neighbouring three carbon atoms are nicely located at the zig-zag edge of the graphite and the two edge carbons next to the graphite-like nitrogen are active for oxygen adsorption, the active site density of Co1000aw is estimated to be 0.29 at.% [44]. Meanwhile, for the 20 wt.% Pt/C, the active site density is estimated to be 0.75 at.%

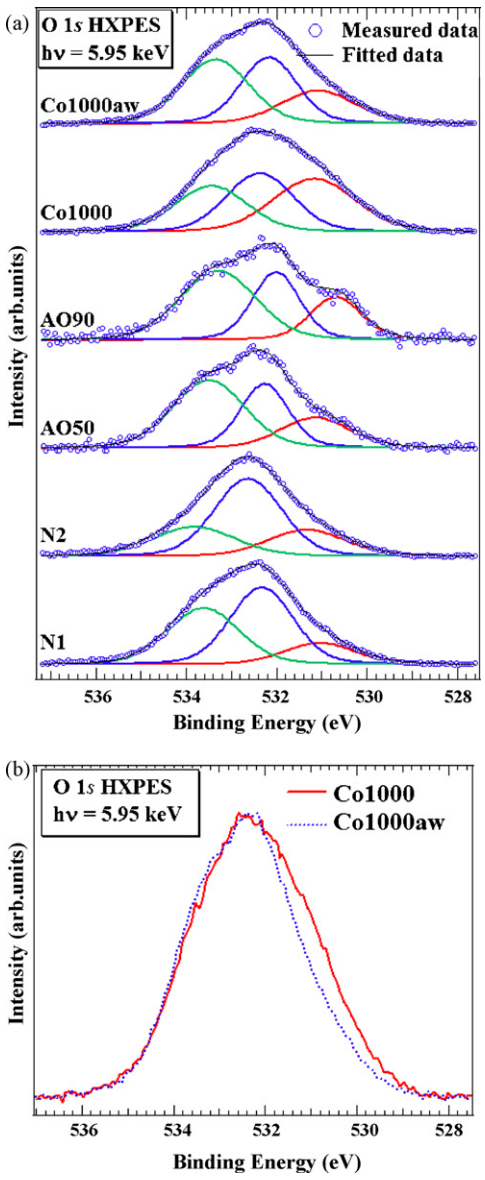

Fig. 5. O 1*s* HXPES spectra of the CACs. (a) The spectra are fitted with Voigt functions followed by the background subtraction with the Shirley method. Red, blue, and green solid lines are C=O groups or non-stoichiometric cobalt oxide (OP1); C–OH and C–O–C groups (OP2); and chemisorbed oxygen or water (OP3) components, respectively. (b) O 1*s* HXPES spectra of nanoshell carbons. (For interpretation of the references to colour in this figure legend, the reader is referred to the web version of the article.)

assuming that half of the Pt atoms in a Pt nanoparticle with a diameter of 2 nm is located on the surface and all of them contribute to the ORR activity [45]. Therefore, the active site density of the CAC is one third of that of Pt/C catalysts. Thus it is important to selectively increase the concentration of graphite-like nitrogen at zig-zag edge for enhancement of the ORR activity.

4. Conclusions

We have investigated the electronic structure of several CACs for PEFCs by HXPES measurements. We have found that acid washing reduces the cobalt concentration in the CACs, but does not change the carbon structure nor the chemical state of nitrogen. Since the cobalt content in the CACs is only 0.03 at.% within the probing depth of the photoelectrons, we suggest that cobalt is not responsible for the ORR activity in the CACs. C 1*s* HXPES spectra suggest the importance of sp^2 carbon network to the ORR activity. From N 1*s* HXPES analysis, we have found that graphite-like nitrogen positively contributes to the ORR activity, which is well consistent with both first-principles simulation [36] and our previous study [35]. There is no correlation between the oxygen content and the ORR activity. The ORR active site density of CAC is estimated to be one third of that of a 20 wt.% Pt/C catalyst, assuming that carbon atom next to graphite-like nitrogen at zig-zag edge is the ORR active site. Thus, by selectively increasing the concentration of graphite-like nitrogen at zig-zag edge in a developed sp^2 carbon network, CACs have the potential to become one of the most promising cathode catalysts without noble metals.

Acknowledgments

This work was performed under Project 08003440-0 at the New Energy and Industrial Technology Development Organization (NEDO). The authors are grateful to HiSOR, Hiroshima Univ. and JAEA/SPring-8 for the development of HXPES at BL15XU of SPring-8.

References

[1] X. Yu, S. Ye, J. Power Sources 172 (2007) 133–144.
[2] R. Jasinski, J. Electrochem. Soc. 112 (1965) 526–528.
[3] M. Lefèvre, E. Proietti, F. Jaouen, J.P. Dodelet, Science 324 (2009) 71–74.
[4] K. Gong, F. Du, Z. Xia, M. Durstock, L. Dai, Science 323 (2009) 760–764.
[5] M. Bron, J. Radnik, M. Fieber-Erdmann, P. Bogdanoff, S. Fiechter, J. Electroanal. Chem. 535 (2002) 113–119.
[6] P. Pylypenko, S. Mukherjee, T.S. Olson, P. Atanassov, Electrochim. Acta 53 (2008) 7875–7883.
[7] C.W.B. Bezerra, L. Zhang, K. Lee, H. Liu, J. Zhang, Z. Shi, A.L.B. Marques, E.P. Marques, S. Wu, J. Zhang, Electrochim. Acta 53 (2008) 7703–7710.
[8] Y. Shao, J. Sui, G. Yin, Y. Gao, Appl. Catal. B: Environ. 79 (2008) 89–99.
[9] R. Bashyam, P. Zelenay, Nature 443 (2006) 63–66.
[10] B. Winther-Jensen, O. Winther-Jensen, M. Forsyth, D.R. MacFarlane, Science 321 (2008) 671–674.
[11] S. Maldonado, K.J. Stevenson, J. Phys. Chem. B 109 (2005) 4707–4716.
[12] P.H. Matter, U.S. Ozkan, Catal. Lett. 109 (2006) 115–123.
[13] P.H. Matter, L. Zhang, U.S. Ozkan, J. Catal. 239 (2006) 83–96.
[14] T. Iwazaki, R. Obinata, W. Sugimoto, Y. Takasu, Electrochem. Commun. 11 (2009) 376–378.
[15] N.P. Subramanian, X. Li, V. Nallathambi, S.P. Kumaraguru, H. Colon-Mercado, G. Wu, J.-W. Lee, B.N. Popov, J. Power Sources 188 (2009) 38–44.
[16] G. Liu, X. Li, P. Ganesan, B.N. Popov, Electrochim. Acta 55 (2010) 2853–2858.
[17] J. Ozaki, N. Kimura, T. Anahara, A. Oya, Carbon 45 (2007) 1847–1853.
[18] Y. Nabae, M. Malon, S.M. Lyth, S. Moriya, K. Matsubayashi, N.M. Islam, S. Kuroki, M. Kakimoto, J. Ozaki, S. Miyata, ECS Trans. 25 (2009) 463–467.
[19] J. Ozaki, S. Tanifuji, A. Furuichi, K. Yabutsuka, Electrochim. Acta 55 (2010) 1864–1871.
[20] Y. Tanabe, E. Yasuda, Carbon 38 (2000) 329–334.
[21] K. Kobayashi, M. Yabashi, Y. Takata, T. Tokushima, S. Shin, K. Tamasaku, D. Miwa, T. Ishikawa, H. Nohira, T. Hattori, Y. Sugita, O. Nakatsuka, A. Sakai, S. Zaima, Appl. Phys. Lett. 83 (2003) 1005–1007.
[22] IMFP is calculated using the TPP-2 M equation in the reference below: S. Tanuma, C.J. Powell, D.R. Penn, Surf. Interface Anal. 17 (1991) 911–926.
[23] J.H. Scofield, Theoretical photoionization cross sections from 1 to 1500 keV, Lawrence Livermore National Laboratory Rep. No. UCRL-51326, 1973.
[24] M. Kobayashi, H. Niwa, Y. Harada, K. Horiba, M. Oshima, H. Ofuchi, K. Terakura, T. Ikeda, Y. Koshigoe, J. Ozaki, S. Miyata, S. Ueda, Y. Yamashita, H. Yoshikawa, K. Kobayashi, J. Phys. Chem. C, submitted for publication.
[25] T. Toda, H. Igarashi, H. Uchida, M. Watanabe, J. Electrochem. Soc. 146 (1999) 3750–3756.
[26] J.R. Pels, F. Kapteijn, J.A. Moulijn, Q. Zhu, K.M. Thomas, Carbon 33 (1995) 1641–1653.
[27] S.C. Ray, C.W. Pao, J.W. Chiou, H.M. Tsai, J.C. Jan, W.F. Pong, R. McCann, S.S. Roy, P. Papakonstantinou, J.A. McLaughlin, J. Appl. Phys. 98 (2005) 033708.
[28] J. Schäfer, J. Ristein, R. Graupner, L. Ley, U. Stephan, Th. Frauenheim, V.S. Veerasamy, G.A.J. Amaratunga, M. Weiler, H. Ehrhardt, Phys. Rev. B 53 (1996) 7762–7774.
[29] R. Haerle, E. Riedo, A. Pasquarello, A. Baldereschi, Phys. Rev. B 65 (2001) 045101.
[30] When high excitation energy such as 5.95 keV is used, an asymmetric broadening of C 1*s* peak is observed due to recoil effects. The broadening of recoil effects does not influence the discussion below because the excitation energy is common among the CAC samples: Y. Takata, Y. Kayanuma, M. Yabashi, K. Tamasaku, Y. Nishino, D. Miwa, Y. Harada, K. Horiba, S. Shin, S. Tanaka, E. Ikenaga, K. Kobayashi, Y. Senba, H. Ohashi, T. Ishikawa, Phys. Rev. B 75 (2007) 233404.
[31] V.A. Coleman, R. Knut, O. Karis, H. Grennberg, U. Jansson, R. Quinlan, B.C. Holloway, B. Sanyal, O. Eriksson, J. Phys. D: Appl. Phys. 41 (2008) 062001.

[32] J. Casanovas, J.M. Ricart, J. Rubio, F. Illas, J.M. Jiménez-Mateos, J. Am. Chem. Soc. 118 (1996) 8071–8076.
[33] J.M. Ripalda, N. Díaz, E. Román, L. Galán, I. Montero, A. Goldoni, A. Baraldi, S. Lizzit, G. Comelli, G. Paolucci, Phys. Rev. Lett. 80 (2000) 2132–2135.
[34] S.E. Rodil, S. Muhl, Diamond Relat. Mater. 13 (2004) 1521–1531.
[35] H. Niwa, K. Horiba, Y. Harada, M. Oshima, T. Ikeda, K. Terakura, J. Ozaki, S. Miyata, J. Power Sources 187 (2009) 93–97.
[36] T. Ikeda, M. Boero, S. Huang, K. Terakura, M. Oshima, J. Ozaki, J. Phys. Chem. C 112 (2008) 14706–14709.
[37] R.A. Sidik, A.B. Anderson, N.P. Subramanian, S.P. Kumaraguru, B.N. Popov, J. Phys. Chem. B 110 (2006) 1787–1793.
[38] M. Fujita, K. Wakabayashi, K. Nakada, K. Kusakabe, J. Phys. Soc. Jpn. 65 (1996) 1920–1923.
[39] D.E. Ramaker, M. Teliska, Y. Zhang, A.Yu. Stakheev, D.C. Koningsberger, Phys. Chem. Chem. Phys. 5 (2003) 4492–4501.
[40] S.S. Yu, W.T. Zheng, Q.B. Wen, Q. Jiang, Carbon 46 (2008) 537–543.
[41] Z.R. Yue, W. Jiang, L. Wang, S.D. Gardner, C.U. Pittman Jr., Carbon 37 (1999) 1785–1796.
[42] B. Briggs, G. Beamson, Anal. Chem. 65 (1993) 1517–1523.
[43] T.J. Chuang, C.R. Brundle, D.W. Rice, Surf. Sci. 59 (1976) 413–429.
[44] The active site density of Co1000aw is calculated as follows: (nitrogen content of Co1000aw; the value is derived from Table 2) × (percentage of graphite-like nitrogen in all nitrogen species; the value is derived from Table 2) × (two carbon atoms at zig-zag edge neighboring graphite-like nitrogen) = 0.37 at.% × 0.395 × 2 = 0.29 at.%.
[45] The active site density of 20 wt.% Pt/C catalyst is calculated as follows: (unit conversion to at.%) × (the half of Pt atoms is on the surface) = 1.51 at.% × 0.5 = 0.75 at.%.